DIRECTIONAL EMISSION FROM ASYMMETRIC RESONANT CAVITIES

Jens U. Nöckel, A. Douglas Stone, Gang Chen, Helene L. Grossman and Richard K. Chang
Department of Applied Physics and Physics, Yale University
P. O. Box 8284, New Haven Connecticut 06520-8284

Published in Optics Letters **21**, 1609 (1996)

ABSTRACT

Asymmetric resonant cavities (ARCs) with highly non-circular but convex cross-sections are predicted theoretically to have high-Q whispering gallery modes with very anisotropic emission. We develop a ray dynamics model for the emission pattern and present numerical and experimental confirmation of the theory.

In recent work [1, 2, 3], a new class of optical resonators has been proposed, comprised of convex dielectric bodies which are substantially deformed from spherical or cylindrical symmetry. We have shown [1, 3] that such asymmetric resonant cavities (ARCs) still retain high-Q ($Q > 1000$) whispering gallery (WG) modes up to distortions as large as 50% of the undeformed radius R; at the same time ray simulations indicated that the emission pattern from these modes becomes highly anisotropic [1]. The initial work focused on cylindrical ARCs; subsequently [2] we generalized the ray dynamics model to explain the experimentally observed directional lasing emission from non-spherical microdroplets. In this work we propose for the first time a general framework for predicting the high-emission directions for ARCs. Although generically the ray dynamics in ARCs is chaotic, by using the Poincaré surface of section method and the adiabatic approximation, it is possible to find universal features in the ray motion which determine the high emission points. Interestingly, the latter do not always coincide with the regions of highest curvature as might be expected. We compare the ray model to the solutions of the wave equation for cylindrical ARCs and to the experimentally determined lasing emission pattern from deformed liquid columns and find good agreement.

The WG modes of *undeformed* spheres or cylinders have high Q because the rays impinge on the boundary with a conserved angle of incidence $\sin\chi > \sin\chi_c \equiv 1/n$, ($n$ is the refractive index) and are thus trapped by total internal reflection. The intrinsic width of these resonances then arises only due to evanescent leakage.

In contrast, in ARCs $\sin\chi$ is not conserved and the dominant escape mechanism is refractive escape: starting from a WG orbit with $\sin\chi > \sin\chi_c$, after a large number of reflections the ray may impinge on the boundary below the critical angle and escape with high probability. The high intensity points in the near-field correspond to the regions where most of the refractive escape occurs; the far-field directionality must be determined by following the bundle of refracted rays.

In order to understand the high emission directions from ARCs, it is essential to analyze the ray dynamics in phase space, and not just by ray-tracing in real space. That is because the partially chaotic (mixed) phase space exhibits remnants of regular structure[1, 2, 3], creating dominant flow patterns which determine the high intensity points. The standard technique used in non-linear dynamics to obtain an understanding of a mixed phase space is the Poincaré surface of section (SOS). It is obtained by plotting, for successive reflections of a ray, the angular position ϕ (azimuthal angle for cylinders, polar angle for spheroids) along the boundary where the reflection occurs, and the value of $\sin\chi$. Recording on the SOS a relatively small number of ray trajectories ($\sim 10-20$) for about 500 reflections yields a detailed picture of the phase space structure. It typically exhibits "islands" and "random" disconnected points, associated with stable and chaotic trajectories, respectively [1, 3]. Certain properties of the SOS are generic for all ARCs and can be used to deduce general features of the escape directionality.

These generic features are illustrated by the ray dynamics of a cylindrical ARC with a 2D quadrupolar deformation of its cross-section (normalized to constant area) given in cylindrical coordinates by

$$r(\phi) = \frac{1}{\sqrt{1+\epsilon^2/2}}\,(1+\epsilon\,\cos 2\phi). \tag{1}$$

The parameter ϵ measures the degree of deformation, the aspect ratio being $(1-\epsilon)/(1+\epsilon) \approx 1-2\epsilon$. For a circle, $\epsilon = 0$; when $\epsilon \geq 0.2$ the shape becomes non-convex and no WG caustics remain in existence [4]. The interesting regime for this shape deformation then lies in the interval $0.05 < \epsilon < 0.15$. Equation (1) describes the simplest 2D ARC because any dipolar component can be removed by a shift of origin, and all other ARCs will involve higher multi-poles. For example, the ellipse (which is the only 2D ARC which has no chaotic trajectories) has multipoles of all even orders although it agrees with the quadrupole to order ϵ.

The partial SOS shown in Fig. 1 is generated for $\epsilon = 0.072$ for which WG trajectories with $\sin\chi < 0.8$ are no longer confined by a caustic and are chaotic; ultimately such orbits will diffuse to lower $\sin\chi$, reach $\sin\chi_c$ and escape refractively. However, if we follow these trajectories for 200 reflections as is done in Fig. 1, they are seen to fall close to curves in the SOS which are given by[5]

$$\sin\chi(\phi) = \sqrt{1-(1-S^2)\,\kappa(\phi)^{2/3}}, \tag{2}$$

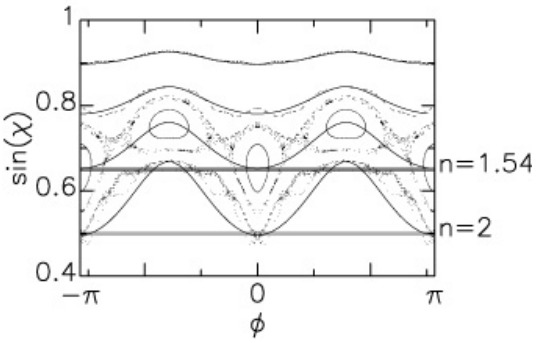

Figure 1: SOS for quadrupole at $\epsilon = .072$, showing four chaotic trajectories followed for 100 - 200 reflections. Superimposed are the curves given by Eq. (2). Shaded horizontal lines indicate $\sin\chi_c$ for different refractive indices n.

where $\kappa(\phi)$ is the curvature of the interface and S is a constant parametrizing the curves, roughly equal to the average value of $\sin\chi$. The relation (2) represents an *adiabatic* approximation valid for $d\kappa/d\phi\sqrt{1-\sin^2\chi} \ll 1$, which describes the ray dynamics for intermediate times rather well, as shown in Fig. 1. It does not describe the *chaotic* behavior of the rays and hence fails badly at long times when the ray will leave the adiabatic curve.

While the failure of the adiabatic approximation for long times must be taken into account in calculating the *broadening* of the resonance due to refractive escape, the approximation is adequate for determining the resonance *frequency* using eikonal theory [6]. In this approach (which neglects broadening) the adiabatic constant S in Eq. (2) can take on only a discrete set of values S_{pm}, where the integers p and m reduce to the radial and azimuthal mode indices, respectively, of the state for circular cross-section. For any deformation ϵ and for any resonance (p, m) we can find the adiabatic invariant curve (AIC) parametrized by S_{pm} along which the corresponding rays move. If this AIC intersects the critical line $\sin\chi_c$, then such resonances are very short-lived and may be ignored. Labeling by S_c the AIC whose minima are tangent to the critical line, the the long-lived WG modes are characterized by $S_{pm} > S_c$. A chaotic trajectory starting at $S = S_{pm}$ eventually deviates from this curve by diffusion with a bias towards smaller S ($\sin\chi$). At each step of this diffusion process a ray moves for intermediate times along a fixed AIC. Ultimately the ray reaches the critical AIC with $S = S_c$ which is tangent to $\sin\chi_c$ and the ray rapidly flows along this AIC to the minima where it escapes refractively with high probability. Therefore assuming that the adiabatic approximation is valid for intermediate times, escape will occur only at or near the tangency points of S_c. [e.g. $\phi = 0, \pi$ for the quadrupole billiard (Fig. 1)]. From Eq. (2) we see that quite generally the minima of the AIC's occur at the point(s) of maximum curvature. Hence this argument suggests that escape occurs primarily near the points of maximum curvature, as might be intuitively expected. Furthermore, because most rays escape from the tangent AIC, they just barely violate

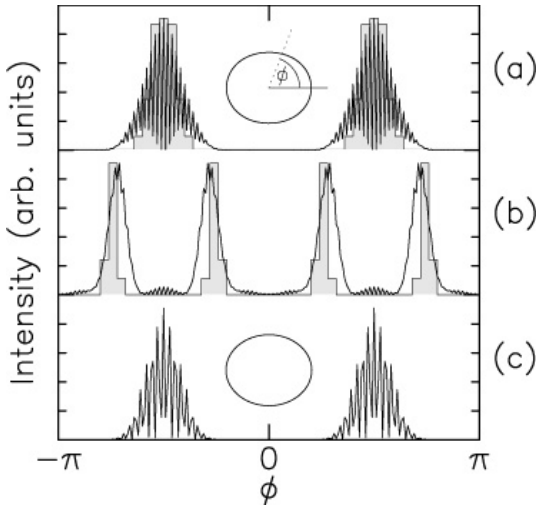

Figure Far-field emission directionality from quadrupole (a,b) and ellipse (c) with distortion $\epsilon = 0.09$, for a resonance $m = 68$. Solid lines: intensity from solution of the wave equation; histograms: classical prediction. The refractive index is $n = 2$ in (a) and $n = 1.54$ in (b,c). The size parameter at this ϵ is $kR = 45.2$ in (a), $kR = 48.1$ in (b) and $kR = 48.0$ in (c). The insets show the shapes.

the total internal reflection condition and are emitted almost tangent to the boundary. The rays are therefore *not* strongly dispersed in angle by refraction, and the emission pattern is peaked in both the near-field *and* far-field, with the far-field emission peaks simply rotated by $\pi/2$.

These conclusions are independent of the particular starting curve S_{pm} as long as it is larger than S_c. Hence we reach the central conclusion of this work: there exists a *universal* and highly directional emission pattern for all WG resonances of cylindrical (2D) ARCs corresponding to $S_{pm} > S_c$. The actual pattern can be generated approximately by simply following a ray ensemble begun on the AIC with $S = S_{pm}$ and making a histogram of the number of rays escaping at a given angular position (near-field) and, after refraction, escaping in a given direction (far-field) [2]. We refer to these as the "classical" directionality histograms.

The resulting far-field directionality is shown in Fig. 2 (a) in comparison with the intensity pattern obtained by exact numerical solution for the quasi-bound state. The good agreement shown is also found for all other resonances studied at this index of refraction. The wave results are obtained by solving for the quasibound states[7] of a deformed cylinder assuming TM polarization. Our algorithm makes use of the Rayleigh hypothesis[8] to expand internal and external fields in Bessel functions, and then imposes appropriate matching conditions at the interface, satisfied for complex wavevector.

Experimental evidence for the universality of the emission directionality can be obtained from a measurement of the lasing emission produced by liquid dye columns.

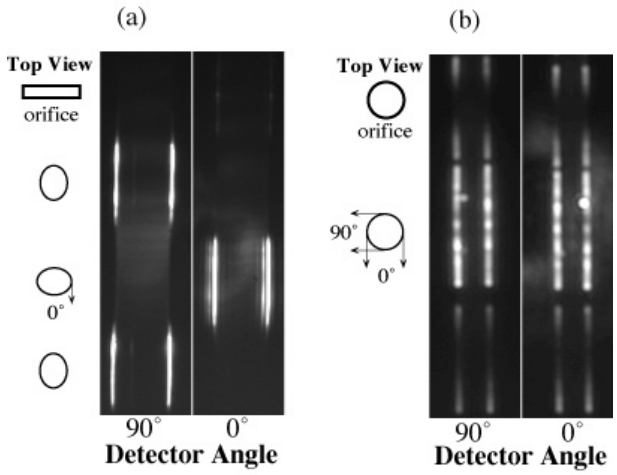

Lasing emission from a liquid dye column created by rectangular (a) and circular (b) orifices. Simultaneous images taken at 0° and 90° angle with respect to the pump beam are shown side by side.

In a variant on the well-studied lasing emission from micro-droplets[2], ethanol containing Rhodamine B dye was forced through circular and rectangular orifices without the usual segmentation of the stream. The dye column produced by the circular orifice (of radius 75μm) is cylindrical, whereas that produced by the rectangular orifice (of dimension 1000μm $\times$ 25μm) has an oval cross-section with an eccentricity which decays (because of viscous damping) until it is nearly circular at 2 cm from the orifice. The cross-sectional distortion which experiences the smallest damping is quadrupolar, so that we expect the dominant deformation to be roughly given by Eq. (1). Hence the dye column at the appropriate height provides a realization of a cylindrical ARC. The surface tension causes the major axis of the quadrupole to oscillate in orientation with respect to the long axis of the orifice.

From previous studies of droplets the lasing of the column should involve many WG modes; however if our universality hypothesis is correct we should still observe highly directional emission from the deformed jet since all such WG modes have the emission pattern of Fig. 2(a). Specifically, we expect to see high emission intensity in the direction perpendicular to the long axis of the deformed cross section which will be rotated by 90° with each half-cycle of the quadrupolar oscillation.

The dye column was pumped with a 537 nm pulsed dye laser with pulse duration $\approx$ 5ns. The pump laser is oriented perpendicular to the long-axis of the rectangular orifice. Two collection lenses set to f/22 were placed at 0° and 90° relative to the pump laser beam. By using mirrors and a beam splitter, lasing images produced by the two lenses were combined side by side on a single CCD detector and were recorded simultaneously with appropriate calibration to preserve spatial correspondence anywhere along the column. As predicted by the theory, we observe [Fig. 3(a)] a striking oscillatory rotation of the high emission intensity between the 90° and 0°

images, commensurate with the oscillation of the deformation of the cross section. No such oscillatory behavior is observed in the lasing emission from the circular liquid column [Fig. 3(b)].

The prediction of emission from the points of maximum κ is based on Eq. (2). However, the actual phase-space flow pattern departs strongly from that predicted by the adiabatic approximation when the AIC intersects large islands of stable motion as can be clearly seen in the SOS of Fig. 1. If the index of refraction is such that $\sin\chi_c$ intersects these large islands at the minima of the AIC, then the relevant trajectories must circulate around these islands. Hence rays escaping at the critical line do not do so at the points of maximum curvature but at two points offset by roughly the width of the island. The resulting near-field pattern is complex due to interference of these two ray bundles, but often shows a *dip* at the points of maximum curvature. Moreover, in all cases the far-field pattern shows strong splitting of the high emission peaks [Fig. 2(b)] in contrast to the two peaks of Fig. 2(a) for both the ray histograms and the exact wave solutions. We refer to this remarkable phenomenon as *dynamical eclipsing*. It deserves further experimental and theoretical study, however the refractive index of $n \approx 1.5$ required for this is not conveniently reached with liquids.

It should be emphasized that the only parameter we changed in order to find the peak-splitting in our calculations is the index of refraction and that the splitting occurs for all resonances we have tested at this index [6]. To confirm further that the numerically determined peak-splitting actually has the classical (ray dynamical) origin we propose, we calculate in Fig. 2(c) the resonances of an elliptical ARC at the same index and aspect ratio as the quadrupole of Fig. 2(b). The ellipse generates no chaos and indeed the adiabatic approximation of Eq. (2) becomes exact. Hence there are no islands near the critical line in the SOS, and we find no peak splitting despite the high similarity between the two shapes in Fig. 2(b),(c). Thus we believe that this phenomenon provides an unambiguous and striking fingerprint of the classical phase space structure in the emission directionality.

We acknowledge partial support by U. S. Army Research Office Grant DAAH04-94-G-0031 and NSF Grant DMR-9215065 and thank Ying Wu and Marko Robnik for helpful discussions.

References

[1] J. U. Nöckel, A. D. Stone and R. K. Chang, Optics Letters **19**, 1693 (1994)

[2] A. Mekis, J. U. Nöckel, G. Chen, A. D. Stone and R. K. Chang, Phys. Rev. Lett. **75**, 2682 (1995)

[3] J. U. Nöckel and A. D. Stone, in: *Optical Processes in Microcavities*, edited by R. K. Chang and A. J. Campillo (World Scientific Publishers, 1996).

[4] J. N. Mather, Ergod. Th. & Dynam. Sys. **2**, 397 (1982)

[5] M. Robnik and M. V. Berry, J. Phys. A: Math. Gen. **18**, 1361 (1985)

[6] J. U. Nöckel and A. D. Stone, unpublished

[7] E. S. C. Ching, P. T. Leung and K. Young, in: *Optical Processes in Microcavities*, edited by R. K. Chang and A. J. Campillo (World Scientific Publishers, 1996).

[8] R. F. Millar, Electron. Lett. **5**, 416 (1969)